

SCIENTIFIC REPORTS



OPEN

Rewiring of neuronal networks during synaptic silencing

Jana Katharina Wrosch¹, Vicky von Einem^{1,2}, Katharina Breininger², Marc Dahlmanns¹, Andreas Maier², Johannes Kornhuber¹ & Teja Wolfgang Groemer¹

Received: 5 June 2017

Accepted: 29 August 2017

Published online: 15 September 2017

Analyzing the connectivity of neuronal networks, based on functional brain imaging data, has yielded new insight into brain circuitry, bringing functional and effective networks into the focus of interest for understanding complex neurological and psychiatric disorders. However, the analysis of network changes, based on the activity of individual neurons, is hindered by the lack of suitable meaningful and reproducible methodologies. Here, we used calcium imaging, statistical spike time analysis and a powerful classification model to reconstruct effective networks of primary rat hippocampal neurons *in vitro*. This method enables the calculation of network parameters, such as propagation probability, path length, and clustering behavior through the measurement of synaptic activity at the single-cell level, thus providing a fuller understanding of how changes at single synapses translate to an entire population of neurons. We demonstrate that our methodology can detect the known effects of drug-induced neuronal inactivity and can be used to investigate the extensive rewiring processes affecting population-wide connectivity patterns after periods of induced neuronal inactivity.

The effects of drug-induced silencing of neuronal activity on the morphology and activity of single synapses have been studied for decades using the voltage-gated sodium channel blocker tetrodotoxin (TTX)^{1–4}. One of the most prominent findings: a strong increase in synaptic excitability^{1–4}. Understanding the consequences of neuronal inactivity has furthered our understanding of synaptic architecture and function over the years and permitted the discovery of activity-independent synaptic processes. Despite Hebbian rules for the use-dependent maintenance of synapses, prolonged inactivity during TTX-treatment induces the expression of additional postsynaptic glutamate receptors^{5,6} and the enlargement postsynaptic densities⁷. Presynaptically, TTX-induced synaptic inactivity induces growth of so-called active zones, characterized by larger numbers of docked vesicles, increased spontaneous release rates, and increases in the number of vesicles released upon a stimulus⁷. Such alterations have been observed in the pathogenesis of tardive dyskinesia⁸, glaucoma⁹, neuropathic pain^{10,11}, and drug addiction^{12–14} and withdrawal^{15,16}. However, it remains unclear whether and how modifications at individual synapses influence the interplay of multiple neurons across a signaling network.

Networks of neurons are studied across many different scales and are generally classified as anatomical, functional, or effective networks depending on the kind of relationship between network nodes that is described by the network edges¹⁷. Anatomical networks describe the physical connections between brain regions or single cells, as shown for example by diffusion tensor magnetic resonance imaging (MRI)^{18–20}, or manual tracings of electron microscopy images^{21–24}. Functional networks describe brain regions or cells that are simultaneously active during resting states^{25,26} or a specific task^{27,28} as for example shown by functional MRI, electroencephalography^{29,30}, or magnetoencephalography^{31,32}. Correlation between time series of the network nodes are used to derive functional networks. Effective networks describe the transmission of information among brain regions or cells as shown for example by multi-electrode array recordings^{33–35}, multi-electrode patch clamping³⁶, and *in vitro*³⁷ and *in vivo*³⁸ calcium imaging. Causal relations between time series of the network nodes are used to derive effective networks.

On the level of single cells, effective networks represent the actual propagation of action potentials. They are the resulting information processing landscape based on synaptic (e.g. post-synaptic excitability) and cellular (e.g. dendritic spine density) characteristics. While the existence of an effective connection between neurons requires at least one synaptic connection between them, the modification of effective connection strength or the loss of a connection may occur independent of synapse formation and loss: synaptic excitability, size of the active zone,

¹Department of Psychiatry and Psychotherapy, Friedrich-Alexander University of Erlangen-Nuremberg, 91054, Erlangen, Germany. ²Pattern Recognition Lab, Department of Computer Science, Friedrich-Alexander University of Erlangen-Nürnberg, 91058, Erlangen, Germany. Correspondence and requests for materials should be addressed to J.K.W. (email: Jana.Wrosch@UK-Erlangen.de)

number of synaptic vesicles and post-synaptic receptor density are only some of the many factors that add up to the effective strength of a connection.

How the network interplay of neurons and brain regions is affected in pathological states has become a focus of basic research. For example, altered functional connectivity of brain regions has been reported in the context of Alzheimer's disease and other types of dementia³⁹, and cognitive improvement in Alzheimer's disease is correlated with a recovery of functional connectivity between the hippocampus and other brain regions⁴⁰. A recent study also shows that amyloid beta peptides, the main components of plaques found in the brains of patients with Alzheimer's disease, directly modulate neuronal network activity⁴¹. Furthermore, functional connectivity throughout the brain is impaired in Parkinson's disease⁴², schizophrenia⁴³ and major depressive disorder^{44–46}. Effective connectivity has been investigated in the context of epilepsy^{35,47} and Sanfilippo syndrome⁴⁸.

Although previous studies on neuronal silencing have described anatomical changes at the level of single synapses, research on population-wide changes in functional or effective connectivity among neurons has been hindered by the lack of a suitable method of network reconstruction. In the past decade, however, several powerful algorithms, such as mutual information⁴⁹, joint entropy⁵⁰, transfer entropy⁵¹, and generalized transfer entropy³⁷, have been proposed, which can be used to investigate neuronal spike time series and to detect correlations between pairs of them. Here, to assess the effects of neuronal silencing on the connectivity of a neuronal network, we developed a method of reconstructing effective connectivity *in vitro* based on statistical spike time analysis of calcium imaging data using a combination of several powerful algorithms and a machine learning approach for the prediction of interconnected neurons.

Results

Neuronal cultures are silenced with tetrodotoxin. We first tested whether the sodium channel blocker tetrodotoxin (TTX) can silence synaptic activity and thus artificially induce effects of neuronal silencing. We measured the intensity of the fluorescence response upon electrical stimulation of Fluo-4 loaded neurons perfused with imaging buffer supplemented with 500 nM or 1 μ M TTX (Fig. 1A,B). The average neuronal response amplitude upon 5 instances of electrical stimulation was reduced to 0.6% of controls \pm 0.4% of controls (SD) during perfusion with 500 nM TTX and to 0.1% of controls \pm 0.5% of controls (SD) during perfusion with 1 μ M TTX (Fig. 1). These results demonstrate that TTX causes synaptic silencing.

To analyze effective connectivity, the culture medium of primary rat hippocampal neurons was supplemented with 500 nM TTX or 1 μ M TTX for 2 days or 1 μ M TTX for 6 days⁷, and in control cultures the medium was supplemented with respective volumes of the solvent sterile water for the same durations. After incubation, neuronal activity was recorded via calcium imaging (Fig. 2A) and subjected to data processing (Fig. 2B). We performed 60 simulations for training and 840 simulations for testing of the classification model, and we recorded and analyzed a total of 75 experiments across the five treatment groups (Table 1). For details on the simulation model and a validation of the classification model please refer to the supplementary Methods and Supplementary Tables ST1 and ST2. Recording, choice of field of view and data analysis were performed blinded to treatment group. Representative recordings of neuronal cultures and the reconstructed effective networks for all treatment groups are shown in Fig. 3.

Tetrodotoxin treatment has no effect on the physical distribution of neurons in culture or their viability. Imaged cells were on average 522 μ m apart from each another, with no difference in distance between connected and unconnected cell pairs. Also, the strength of formed connections was independent of the connection distance (Supplementary Figure S1). As expected⁵², dissociated hippocampal neurons connected with negative assortativity in all treatment groups (Supplementary Figure S2). The viability of the neuronal cultures did not suffer from the TTX treatment compared to controls (Supplementary Figure S3).

After neuronal silencing the effective connection strength between neurons is increased. We set out to test, if - additional to the molecular and cellular mechanisms of increased synapse size, vesicular release probability, and neuronal excitability after neuronal inactivity⁷ - there is also an increase in effective connection strength in the neuronal cultures. Using statistical spike time analysis to reconstruct effective connectivity, we examined the probability of propagation of action potentials from one cell to another across the culture (Fig. 4A,B). We found that TTX-induced silencing of neuronal activity for 2 or 6 days increased the propagation probability by approximately 2-fold (Fig. 4C), suggesting that synaptic modifications, such as increased vesicular release probability translate into stronger connections between cells on a population level.

Neuronal cultures undergo rewiring during activity silencing. When analyzing the structure of the neuronal networks, it appeared not only that the strength of connections between cells was increased but also that the network contained more connections. An additional connection can be established by a synapse formation between two neurons that were not previously synaptically connected. The strengthening of a connection however can be established also by the formation of additional synapses between already connected neurons or by a strengthening of already existing synapses between the two cells. More connections in a network can be quantified in different ways: One parameter is the connectivity degree, which is the number of effective connections normalized to the number of cells in the network. Another parameter, the clustering coefficient, provides information about the distribution of connections. High clustering coefficients appear in networks, in which a cell's connection partners are also tightly connected with each other (Fig. 5A,B). We found that TTX-induced silencing of neuronal activity for 2 or 6 days approximately doubled both the connectivity degree and the clustering coefficient (Fig. 5C,D).

A third way to characterize the number of connections of a network is the characteristic path length, which describes the average distance between two cells in a network (with "distance" being defined as the sum of

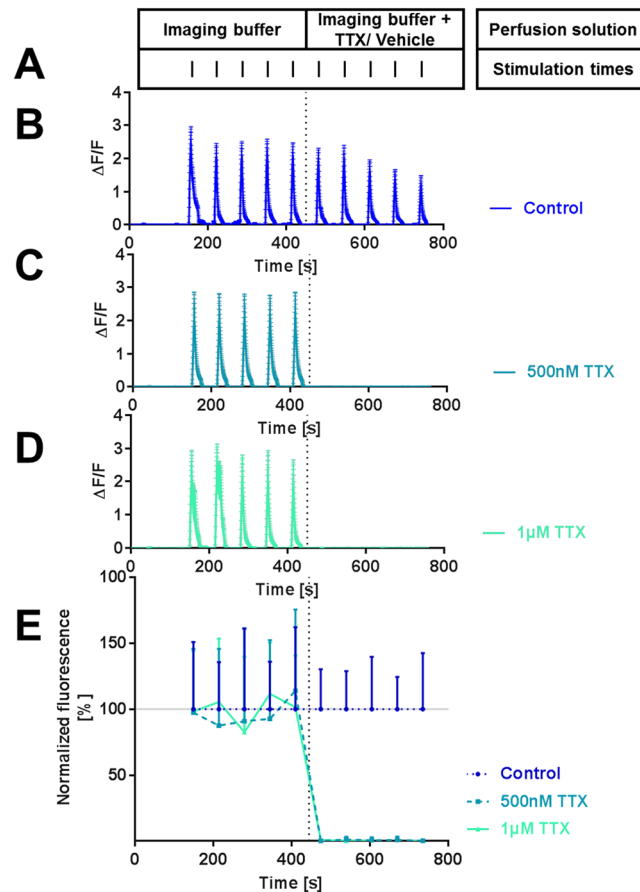


Figure 1. TTX-induced silencing of neuronal responses. TTX blocked neuronal responses as shown by Fluo-4, a calcium-sensitive fluorescent activity marker. Vertical bars indicate time points of electrical stimulation. The dashed line marks the time of perfusion solution switch. **(A)** Scheme of experimental procedure. **(B–D)** Representative recording traces (mean with standard deviation). Electrical stimulation with 50 pulses produced robust signals with a high signal-to-noise ratio. **(E)** Time course of Fluo-4 fluorescence signals normalized to the responses in the control condition for each of the 10 pulses (mean and standard deviation). Numbers of analyzed cells with the numbers of independent recordings in parenthesis: control: 399 (6), 500 nM TTX: 571 (8), 1 μ M TTX: 644 (11). Similar to those in the connectivity experiments, the cultures were recorded at age DIV 14.

intermediate steps in the shortest path between cells). In a network with many connections, paths between two cells tend to be relatively direct, resulting in a short characteristic path length. In a more sparsely connected network, however, the most direct path between two cells requires a number of intermediate steps, resulting in a longer characteristic path length. Details and formulas to calculate the topology measures can be found in the Supplementary Methods. This characteristic path length of the control networks were 2.02 (mean of 2 day controls \pm 0.28 standard deviation) and 2.19 (mean of 6 day controls \pm 0.50 standard deviation), which indicates a network in which almost every cell is directly connected to every other cell (characteristic path length of 1). The additional connections in TTX treated cultures as seen in the connectivity degree did form at sites in the network that only slightly decreased the characteristic path length (Fig. 5E). When investigating effective (or functional) networks one can also calculate the weighted characteristic path length⁵³. This measure represents also the sum of intermediate steps of the shortest paths in the network but each intermediate connection is weighted by the respective connections strength. The weighted characteristic path length represents a combined measure of connection number and connection strengths. We found that TTX-induced silencing of neuronal activity for 2 or 6 days reduced the weighted characteristic path length by approximately half (Fig. 5F), demonstrating the extent of rewiring and connection strengthening during neuronal silencing.

Transmission efficiency is enhanced in tetrodotoxin treated neuronal cultures. Using the method of reconstructing the effective network of an entire population of neurons, we observed stronger connections and an increased number of connections after the silencing, resulting in a network twice as dense with effective connections as its original state. The outcome of these two processes can be quantified as the signal transmission efficiency across the network⁵³ (Fig. 6A,B). This measure describes how the combination of number of connections and their individual strengths combine to form the actual information processing landscape of the network. We found that the combination of both silencing effects boosted the global transmission efficiency by nearly 4-fold (Fig. 6C). Such a potentiation of synaptic communication in previously silenced neuronal cultures

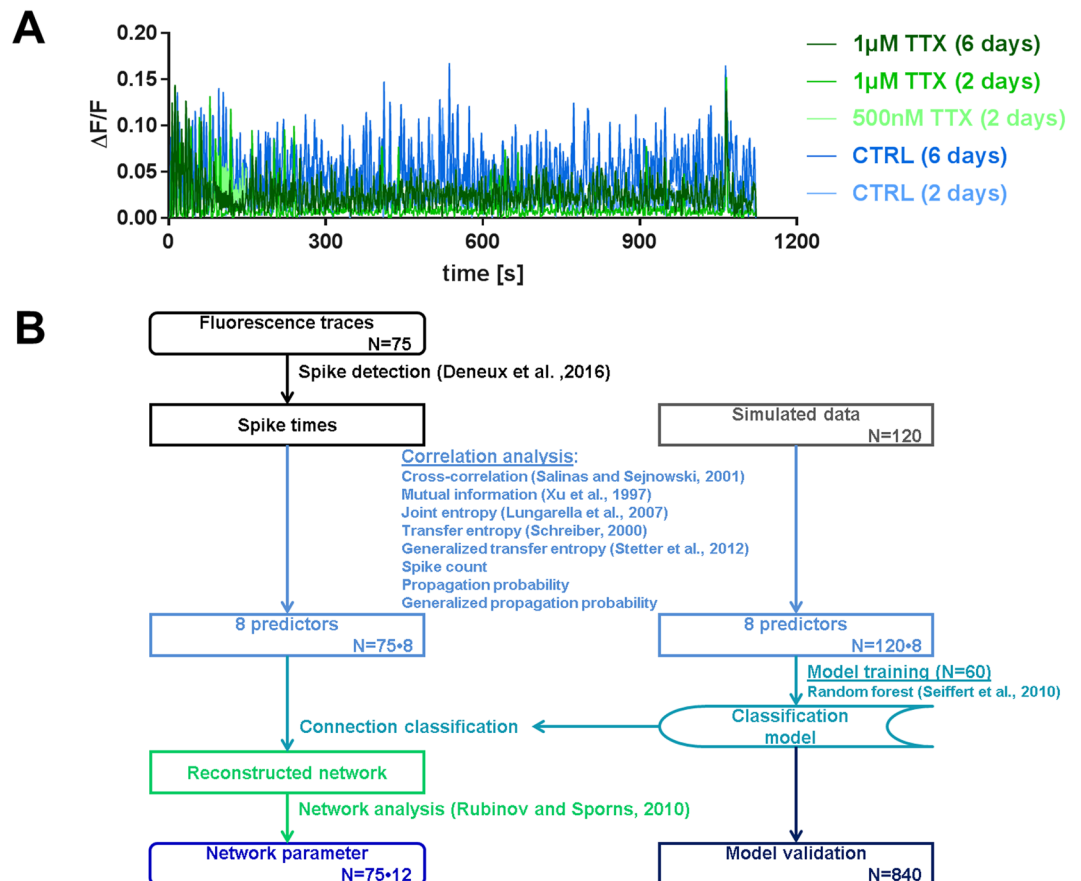


Figure 2. Representative neuronal activity recordings and data processing flow. (A) Typical fluorescence time course obtained from Fluo-4 calcium imaging of spontaneous activity of a culture treated with 500 nM TTX, 1 μM TTX or the same volume of the solvent water (control) for two or six days. (B) Flow chart of the data processing routine used to reconstruct effective neuronal networks and to obtain network parameters with the number of analyzed recordings and simulations. Annotated names refer to references as cited in the main text.

may most likely be an effect of increased action potential propagation probability and possibly the growth of new connections.

Taken together, these results show that the silencing of neuronal activity not only increases action potential propagation across connections but also leads to the formation of many additional effective connections.

Discussion

Our observations confirm previous reports that the silencing of neuronal activity over a short time span potentiates the strength of synaptic connections. However, whereas earlier studies only show that neuronal inactivity induces changes at the level of individual synapses, including increased synapse size and postsynaptic receptor concentration^{5–7}, our study demonstrates that neuronal silencing increases action potential propagation probability across an entire neuronal network. In addition, we discovered reduced neuronal activity not only increased synaptic sensitivity⁷ but also a largely increased number of connections throughout the network.

The ability to detect differences in connectivity patterns is an important first step towards understanding how unused neurons become reconnected, such as during the recovery of stroke patients. Research in this area has generated an extensive body of evidence supporting the hypothesis that recovery from stroke reflects the recovery of connectivity of “silenced” brain regions^{54–59}. A deeper understanding of this process could help to accelerate the recovery of functional connections not only in stroke patients but also in those with spatial neglect^{60,61}, traumatic brain injury^{62,63}, or glioma⁶⁴. A deeper knowledge of this rewiring process also provides new insight into the sprouting of new dendritic spines during neuronal silencing⁶⁵, which has long been observed but not explained.

Neuronal cultures, silenced for 6 days, exhibited reduced strengthening and formation of synaptic connections and less potentiation of synaptic transmission compared with those silenced for 2 days with the same TTX concentration of 1 μM . This suggests that the potentiating effects of neuronal silencing compete against the opposing loss of connections, leading to the weakening and ultimately to the loss of effective connections with more prolonged inactivity.

These effects occurred without an impairment of cell viability after the pharmacological treatment (Supplementary Figure S3). Also the overall synchrony of the neuronal activity in the culture was unaffected by the treatment (Supplementary Figure S4). The causal relation between different cells’ time series that we measured

Simulations	
Classification training data	
Number of simulations	60
Connectivity degree ³	20.1% ± 5.0%
Propagation probability ³	3.9% ± 0.9%
Number of cells per simulation ³	43 ± 0
Classification test data	
Number of simulations	840
Connectivity degree	5–80%
Propagation probability	5–80%
Number of cells per simulation	30–101
Recordings	
Control group, 2 days incubation	
Treatment	2 days incubation with according volume of water
Number of recordings ¹	11 (12)
Culture age at recording ²	DIV 12–17
Connectivity degree ³	21.1% ± 7.0%
Propagation probability ³	19.6% ± 10.1%
Number of cells per recording ³	34.9 ± 17.4
Control group, 6 days incubation	
Treatment	6 days incubation with according volume of water
Number of recordings ¹	18 (18)
Culture age at recording ²	DIV 13–15
Connectivity degree ³	19.6% ± 12.3%
Propagation probability ³	14.5% ± 5.2%
Number of cells per recording ³	44.5 ± 13.2
Silencing group, 2 days incubation	
Treatment	2 days incubation with 500 nM TTX
Number of recordings ¹	16 (22)
Culture age at recording ²	DIV 12–17
Connectivity degree ³	37.2% ± 27.1%
Propagation probability ³	45.9% ± 21.2%
Number of cells per recording ³	40.6 ± 21.5
Silencing group, 2 days incubation	
Treatment	2 days incubation with 1 μM TTX
Number of recordings ¹	13 (15)
Culture age at recording ²	DIV (13–15)
Connectivity degree ³	45.1% ± 20.4%
Propagation probability ³	37.1% ± 20.5%
Number of cells per recording ³	43.1 ± 18.6
Silencing group, 6 days incubation	
Treatment	6 days incubation with 1 μM TTX
Number of recordings ¹	17 (23)
Culture age at recording ²	DIV 13–15
Connectivity degree ³	24.2% ± 15.7%
Propagation probability ³	34.5% ± 12.1%
Number of cells per recording ³	49.2 ± 28.5

Table 1. Basic descriptive statistics for all simulations and neuronal recordings. ¹The numbers of recordings are shown as analyzed recordings (total number of conducted experiments). Recordings with less than 30 active neurons were excluded from the analysis. ²DIV = day *in vitro*. ³Connectivity degree, propagation probability and number of cells per simulation/ recording are shown as mean ± standard deviation.

as effective connection strengths, however, showed the reported increase after TTX treatment. Additional evidence supporting the hypothesis of competing connection strengthening and connection loss comes from a more detailed analysis of neuronal network structure. With the disappearance of alternative routes of communication

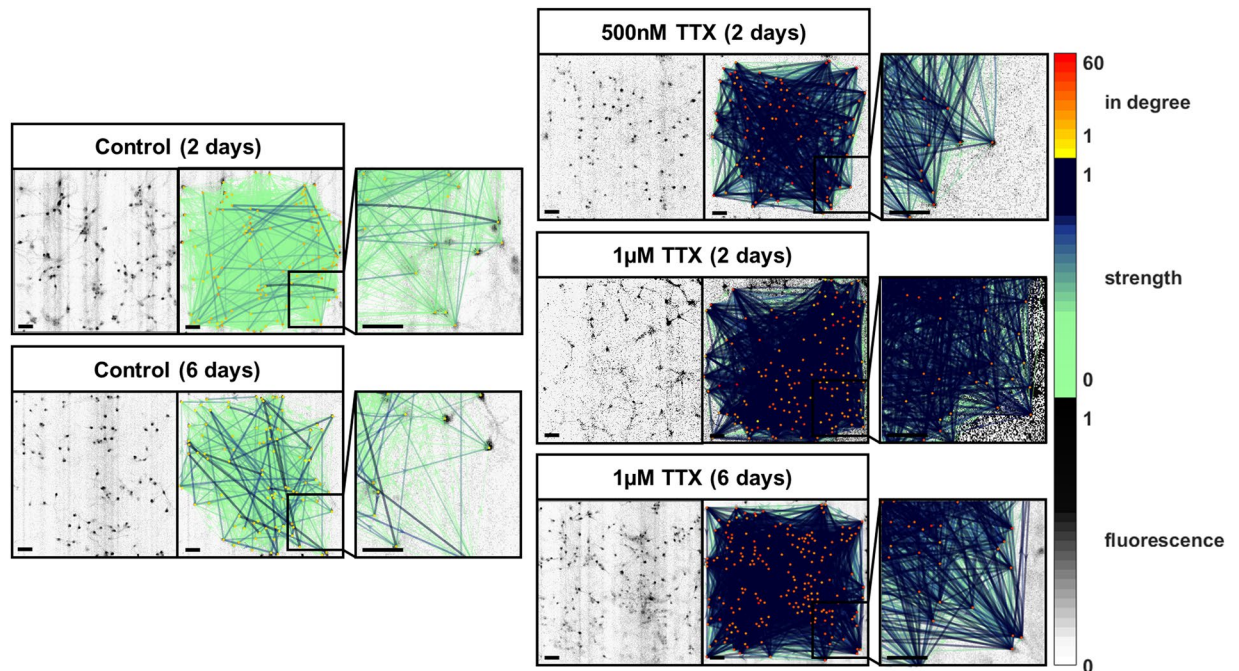


Figure 3. Representative images of effective network reconstruction with connection strengths after TTX-induced silencing for 2 or 6 days. The panels show network plots with color-coded number of incoming connections (in degree) and connection strength (weight). Connection strength is represented by thin, light arrows if low and thick, dark arrows if high. The treatment of neuronal cultures with 500 nM TTX or 1 μ M TTX for two or six days yielded effective networks with more connections and higher connection strengths. Scale bars = 100 μ m.

among cells after 6 days of TTX-induced silencing, the betweenness centrality of cells with remaining connections increased (Supplementary Figure S5). The number of incoming and outgoing connections, which is increased after two days of silencing normalized back to the original values after six days of treatment with the same TTX concentration (Supplementary Figure S6). This is in line with the previously described reduction of dendritic arborization and length after longer-term synaptic inactivity⁶⁶. Understanding how to shift this counterbalance toward the densification of neuronal networks and the strengthening of connections might facilitate the development of treatment options for a wide range of diseases such as multiple sclerosis^{67,68}, Alzheimer's disease^{39,41,69}, mood disorders^{70–72}, and addiction⁷³.

Although neurons may have appeared to make indiscriminant connections to retain synaptic transmission during network silencing, the connections were not formed at random. Rather, the maintenance of a constant out-per-in-degree and modularity during neuronal inactivity (Supplementary Figure S7) point toward an action potential-independent regulatory mechanism. A previous study shows that neurons maintain their distribution of different synapse types under TTX treatment⁶⁶. Such basic network properties could be maintained in the absence of neuronal firing through signaling between axons and synaptic terminals or communication via spontaneous synaptic vesicle release^{74,75}, although further research on this topic is needed.

In summary, using a novel methodological approach, we uncovered the formation of new effective connections during short-term (2 days) but not long-term (6 days) silencing of neuronal activity. This approach opens the field for further research on population-wide effects of different pharmacological substances and implicates neuronal connectivity as a possible drug target in neurological and psychiatric diseases.

Materials and Methods

General methods. We followed the Standards for Reporting Diagnostic Accuracy Studies (STARD)⁷⁶ adapted to our study design in accordance with recommendations for good scientific practice by the German Research Foundation⁷⁷. All chemicals were obtained from Invitrogen (Carlsbad, CA) unless stated otherwise. The incubation wells for the different experimental groups were randomly assigned and imaging and image processing were conducted blinded to the experimental condition to avoid expectation bias when choosing a field of view for imaging or parameters for data analysis.

Code availability. Image processing and analysis, as well as network reconstruction and analysis, were carried out using original scripts in MATLAB (RRID: SCR_001622, Mathworks Inc., Natick, MA). Graph theoretical network analysis was performed using the subfunctions provided in the Brain Connectivity Toolbox by Rubinov *et al.* (RRID: SCR_004841)⁵³. All scripts used to generate data are available in the GitHub repository (www.github.com/janawrosch/effective_connectivity). The box-and-whiskers plots were generated with the Graph Pad Prism software (La Jolla, CA).

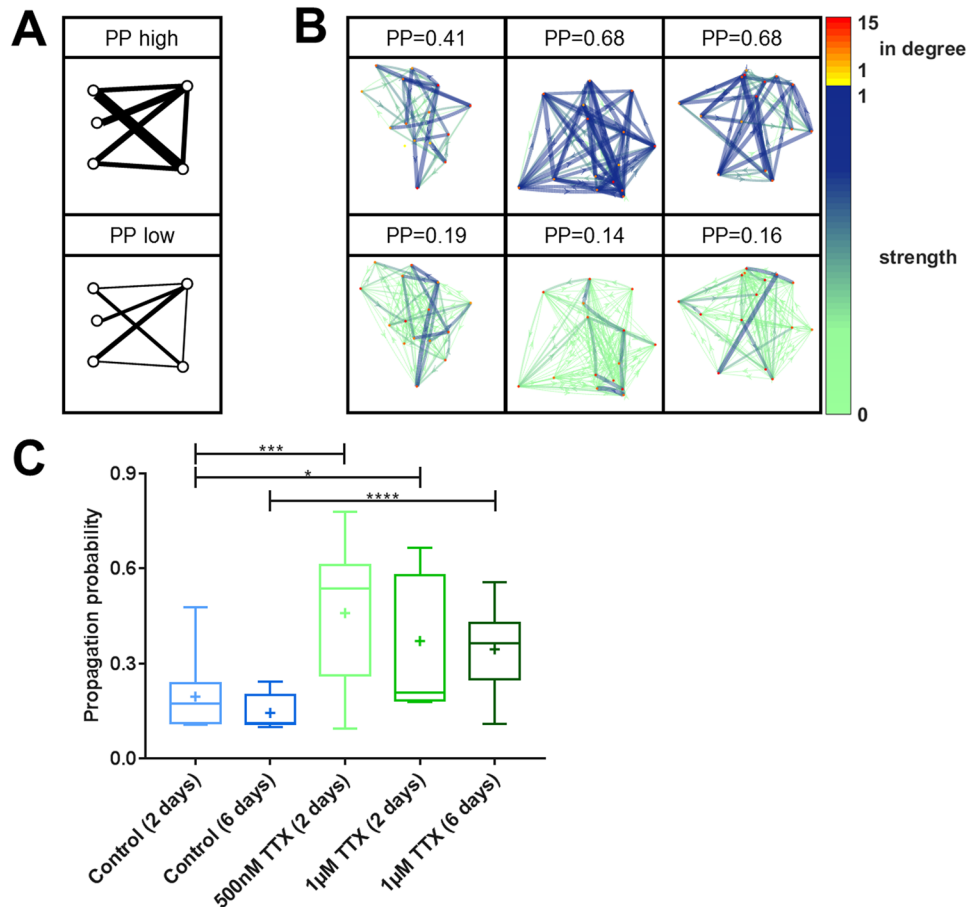


Figure 4. Enhanced propagation probability across a neuronal network after TTX-induced silencing. **(A)** Schematic illustration of high and low propagation probability (PP) in a network. **(B)** Visualization of 15-cell networks with different PP. Weak connections are shown as thin, light arrows, and strong connections are shown as dark, thick arrows. The in-degree – the number of incoming connections – of each node is color-coded. **(C)** After TTX treatment PP is significantly increased (control (2 days) vs. 500 nM TTX (2 days): $p = 0.001$, control (2 days) vs. 1 μM TTX (2 days): $p = 0.019$, control (6 days) vs. 1 μM TTX (6 days): $p < 0.001$, two-sided t-tests). Numbers of experiments: control (2 days): 11, control (6 days): 18, 500 nM TTX (2 days): 16, 1 μM TTX (2 days): 13, 1 μM TTX (6 days): 17. The boxes extend from the 25th to the 75th percentiles. The median and mean are shown as horizontal lines and crosses, respectively. The whiskers show the range of values.

Data availability. Detailed tables of the data and inferential statistics can be found in the Supplementary Excel-Item. Other data are available from the corresponding author per request at any time.

Cell culture. Primary hippocampal neurons were obtained as previously described^{78,79}. Briefly, hippocampi were removed from 1- to 3-day-old Wistar rats of any sex (RRID: RGD_68115, Charles River, Wilmington, MA) after sacrifice in accordance with guidelines of the State of Bavaria and with approval by the ethics committee of the Friedrich-Alexander University of Erlangen-Nürnberg. Hippocampal cells were washed, digested, dissociated, and centrifuged. The cell pellet was resuspended in medium, and cells were plated on glass coverslips in a 12-well plate coated with MatrigelTM (BD Biosciences, San Jose, CA). After a medium change on day 2 *in vitro* (DIV 2), cells were incubated until use in experiments. We conducted 75 experiments with 75 different coverslips that were seeded in 43 independent preparations. The preparations were conducted on different days from groups of 6 animals, each.

Pharmacological treatments. Experimental cell cultures were treated with 500 nM or 1 μM TTX (Sigma-Aldrich, CAS 4368-28-9, St. Louis, MO) for 2 days or with 1 μM TTX for 6 days. TTX was diluted in sterile water. Control cell cultures were treated with the respective volumes of sterile water for the same durations. These TTX concentrations and incubation times were used in a previous major study of synaptic disuse⁷. The culture medium was supplemented with TTX or sterile water on the according number of days before the imaging experiments, which were conducted on DIV 12–17.

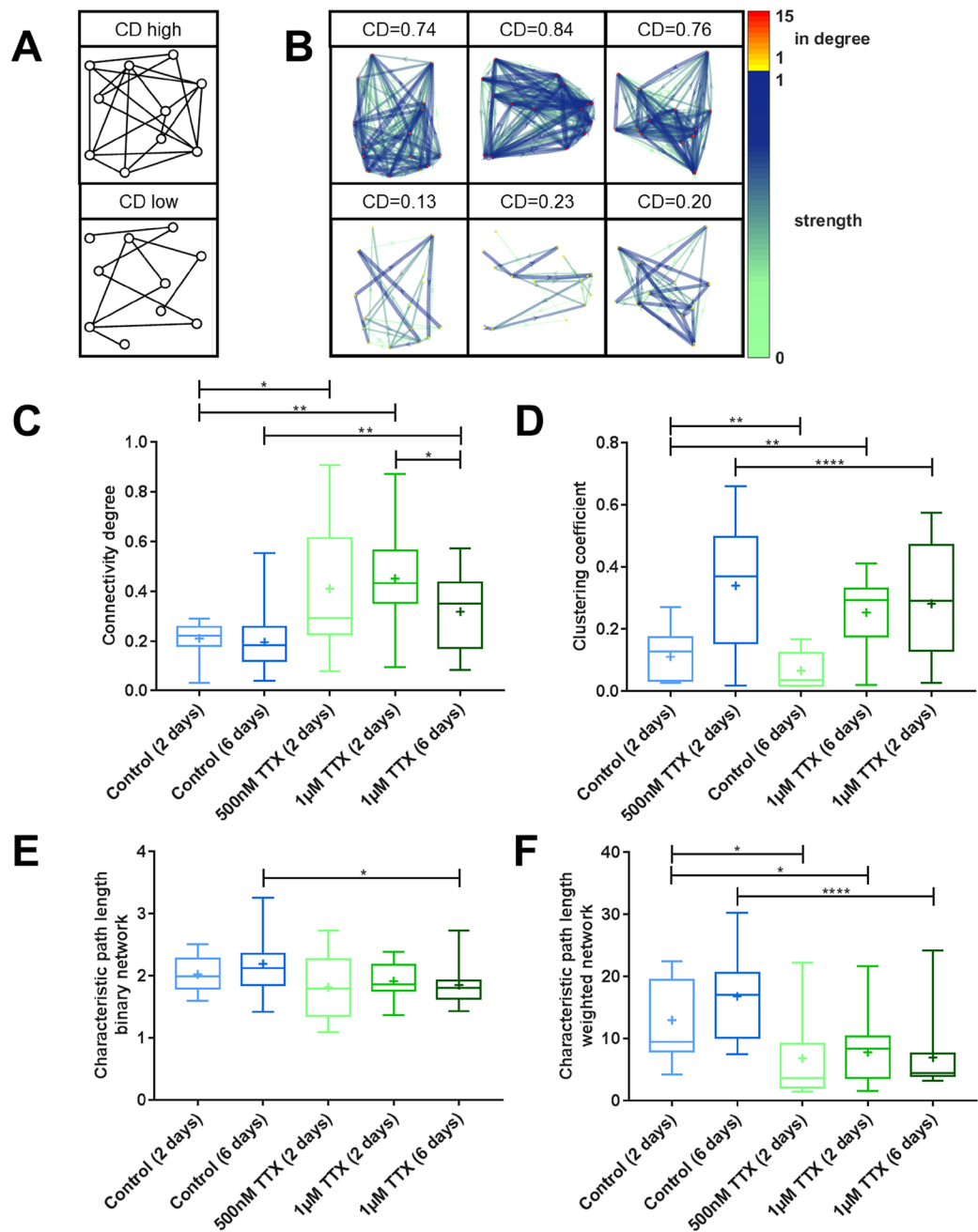


Figure 5. Increased number of connections in neuronal networks after TTX-induced silencing. (A) Schematic illustration of networks with high and low connectivity degree (CD), high and low clustering coefficients, and low and high characteristic path length, respectively. (B) Visualization of 15-cell networks with different CD. Weak connections are shown as thin, light arrows, and strong connections are shown as dark, thick arrows. The in-degree – the number of incoming connections – of each node is color-coded. (C) After TTX treatment the connectivity degree was significantly increased (control (2 days) vs. 500 nM TTX (2 days): $p = 0.021$, control (2 days) vs. 1 μ M TTX (2 days): $p < 0.001$, control (6 days) vs. 1 μ M TTX (6 days): $p = 0.010$, two-sided t-tests). (D) The clustering coefficient was significantly increased after TTX-induced silencing (control (2 days) vs. 500 nM TTX (2 days): $p = 0.003$, control (2 days) vs. 1 μ M TTX (2 days): $p = 0.008$, control (6 days) vs. 1 μ M TTX (6 days): $p < 0.001$, two-sided t-tests). (E) The already low characteristic path length was not significantly lowered after 500 nM or 1 μ M TTX treatment for 2 days but after six days of 1 μ M TTX treatment (control (2 days) vs. 500 nM TTX (2 days): $p = 0.232$, control (2 days) vs. 1 μ M TTX (2 days): $p = 0.364$, control (6 days) vs. 1 μ M TTX (6 days): $p = 0.027$, two-sided t-tests). (F) After TTX-induced silencing the characteristic path length of the weighted network, which is a combined measure of connection number and connection strength was significantly reduced (control (2 days) vs. 500 nM TTX (2 days): $p = 0.032$, control (2 days) vs. 1 μ M TTX (2 days): $p = 0.044$, control (6 days) vs. 1 μ M TTX (6 days): $p < 0.001$, two-sided t-tests). Numbers of experiments: control (2 days): 11, control (6 days): 18, 500 nM TTX (2 days): 16, 1 μ M TTX (2 days): 13, 1 μ M TTX (6 days): 17. The boxes extend from the 25th to the 75th percentiles. The median and mean are shown as horizontal lines and crosses, respectively. The whiskers show the range of values.

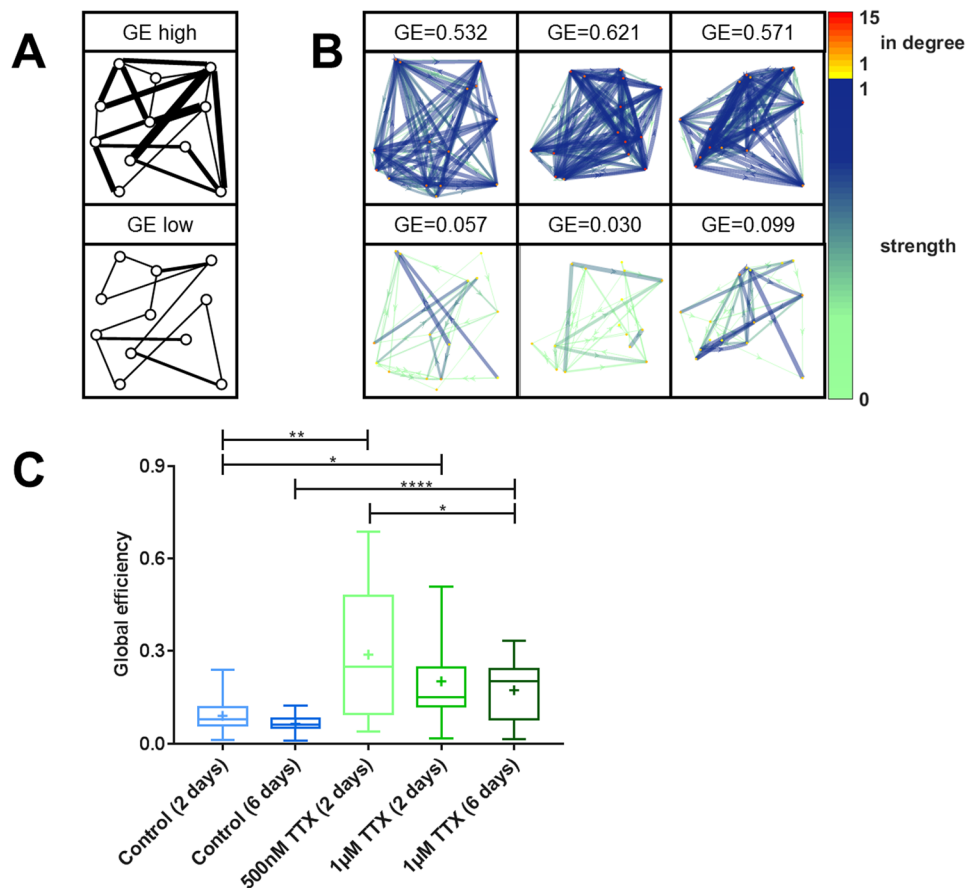


Figure 6. Potentiated signal transmission efficiency after TTX-induced silencing. **(A)** Schematic illustration of networks with high and low global efficiency (GE). **(B)** Visualization of 15-cell networks with different GE. Weak connections are shown as thin, light arrows, and strong connections are shown as dark, thick arrows. The in-degree – the number of incoming connections – of each node is color-coded. **(C)** After TTX treatment GE was significantly enhanced (control (2 days) vs. 500 nM TTX (2 days): $p = 0.007$, control (2 days) vs. 1 μM TTX (2 days): $p = 0.027$, control (6 days) vs. 1 μM TTX (6 days): $p < 0.001$, two-sided t-tests). Numbers of experiments: control (2 days): 11, control (6 days): 18, 500 nM TTX (2 days): 16, 1 μM TTX (2 days): 13, 1 μM TTX (6 days): 17. The boxes extend from the 25th to the 75th percentiles. The median and mean are shown as horizontal lines and crosses, respectively. The whiskers show the range of values.

Cell viability: LDH-assay. Cell viability after the pharmacological treatments was assessed with a lactate-dehydrogenase-assay (Promega Cyto Tox 96 Non-Radioactive Cytotoxicity Assay (Madison, WI)) according to manufacturer instructions: The supernatant of 5 different cultures was collected for each condition. Additionally, the supernatant of two different lysed cultures and a sample of pure medium were collected. The samples were analyzed in triplicates. Each sample was incubated with the same volume of substrate-buffer-mix (containing lactate and tetrazolium) for 30 minutes at room temperature and the reaction was stopped with the same volume of stop-solution. The color change yielded by the conversion of tetrazolium to red formazan with NADH available from the enzymatic activity of lactate-dehydrogenase was quantified with a BioRad Benchmark Photometer (Hercules, CA) at 490 nm in a flat-bottom 96-well plate three times and averaged. The ratio of cytotoxicity was calculated according to manufacturer instructions:

$$[\% \text{ cytotoxicity}] = \frac{[\text{measured LDH release}]}{[\text{maximum LDH release (lysis)}]} \cdot 100$$

Live cell recording of neuronal activity for network reconstruction. To ensure adequate cell health, samples were chosen after bright field microscopy inspection, excluding coverslips that showed signs of weak vitality (e.g., no dense soma or detached, loose axons). Detailed descriptions of the staining process and the experimental setup are provided in the Supplementary Methods. Briefly, cultures were stained with the calcium-sensitive fluorescent dye Fluo-4-AM, washed with phosphate-buffered saline, and placed into an imaging chamber filled with imaging buffer. Recordings were made at room temperature on a Nikon TI-Eclipse inverted fluorescence microscope equipped with a 10 \times , 0.45 NA objective (Nikon Instruments Europe, Düsseldorf,

Germany) and a water-cooled EM-CCD camera (iXon Ultra 897, Andor, Belfast, Northern Ireland). For each recording, we captured 18.5 min of spontaneous activity, which is sufficient to allow network reconstruction with maximal accuracy (Supplementary Figure S8A). After recording spontaneous activity, we delivered a 1200-pulse electrical field stimulation train of 40 Hz for the automatic detection of responsive regions of interest, delivered at alternating polarity through two parallel platinum electrodes spaced 10 mm apart. Images were recorded using Andor Solis software with an exposure time of 1 ms and a recording frame rate of 27.33 Hz, resulting in 31156 frames per recording. Recordings were exported into tagged image file format containing 512×512 pixels of 16-bit monochromatic intensity values.

TTX-induced silencing of neuronal activity. To achieve neuronal silencing through TTX application, cells were prepared as described above and imaged using the same experimental setup with the addition of a fast-step perfusion system (Warner Instruments, Hamden, CT). After cells acclimated to perfusion for 2:30 min, they were repeatedly stimulated with 10 trains of 50 1-ms pulses of alternating polarity at 10 Hz with a 60-s inter-stimulation interval. During the first phase of the experiment (i.e., the first five stimulations, 445 s), cells were perfused with plain imaging buffer. During the second phase of the experiment (i.e., the second five stimulations, 325 s), cells were perfused with imaging buffer supplemented with 500 nM TTX, 1 μ M TTX, or equivalent volumes of sterile water. We recorded the fluorescence increase of the cells in response to the electrical stimulations. Each cell's ten response amplitudes were normalized to the average response amplitudes in the used control condition.

Image processing and network reconstruction. A detailed description of the image processing and network reconstruction steps is provided in the Supplementary Methods. Briefly, images were filtered according to the fluorescence increase upon electrical stimulation, ensuring the detection of only viable neuronal cells, and regions of interest (i.e., neuronal cell bodies) were detected using a feature point detection algorithm⁸⁰. The fluorescence signal was extracted from the image stacks and the relative fluorescence $\Delta F/F$ was derived as previously described⁸¹. Underlying action potentials were inferred from the relative fluorescence traces using an extended template fitting spike estimation algorithm⁸². The gained spike trains for each cell were analyzed to determine similarity and causal relations between all possible pairs of cells with eight different methods: simple cross-correlation⁸³, mutual information⁴⁹, joint entropy⁵⁰, transfer entropy⁵¹, generalized transfer entropy³⁷, spike count, propagation probability and generalized propagation probability. A detailed description of the used algorithms can be found in the Supplementary Methods. The resulting eight values for each pair of cells were then used as predictors in a random undersampled adaptive boosted random forest classification model⁸⁴ to determine which cell pair's causal links were strong enough to be classified as connected. This classification may err so the sensitivity, specificity and accuracy of the classification were validated on simulations with a wide range of initial parameters and the same time resolution as the *in vitro* imaging data (Supplementary Table ST1). On simulated test data with parameters similar to those of the classification training data the model classified with an accuracy of 91.1%, sensitivity of 77.8% and specificity of 93.3% (Supplementary Figure 8C).

Network analysis. Reconstructed effective networks were analyzed using the predicted connection strength as the connection weight. From a multitude of possible network topology properties⁵³, we chose to analyze 12 different features that can be transferred to an underlying biological rationale. Detailed mathematical descriptions of the network topology parameters are found in the Brain Connectivity Toolbox documentation by Rubinov *et al.* (RRID: SCR_004841)⁵³ and in the Supplementary Methods. Detailed descriptive and inferential statistics for each network parameter are provided as the Tables in the Supplementary Excel-Item.

References

- Cannon, W. B. A law of denervation. *The American Journal of the Medical Sciences* **198**, 737–749 (1939).
- Sharpless, S. K. Reorganization of Function in the Nervous System—Use and Disuse. *Annual review of physiology* **26**, 357–388, doi:<https://doi.org/10.1146/annurev.ph.26.030164.002041> (1964).
- Sharpless, S. K. Supersensitivity-like phenomena in the central nervous system. *Federation proceedings* **34**, 1990–1997 (1975).
- Burke, W. & Hayhow, W. R. Disuse in the lateral geniculate nucleus of the cat. *The Journal of physiology* **194**, 495–519 (1968).
- Turrigiano, G. G., Leslie, K. R., Desai, N. S., Rutherford, L. C. & Nelson, S. B. Activity-dependent scaling of quantal amplitude in neocortical neurons. *Nature* **391**, 892–896, doi:<https://doi.org/10.1038/36103> (1998).
- Lissin, D. V. *et al.* Activity differentially regulates the surface expression of synaptic AMPA and NMDA glutamate receptors. *Proceedings of the National Academy of Sciences of the United States of America* **95**, 7097–7102 (1998).
- Murthy, V. N., Schikorski, T., Stevens, C. F. & Zhu, Y. Inactivity produces increases in neurotransmitter release and synapse size. *Neuron* **32**, 673–682 (2001).
- Casey, D. E. Tardive dyskinesia: pathophysiology and animal models. *The Journal of clinical psychiatry* **61**(Suppl 4), 5–9 (2000).
- Clark, C. V. Autonomic denervation hypersensitivity in the primary glaucomas. *Eye* **3**(Pt 3), 349–354, doi:<https://doi.org/10.1038/eye.1989.50> (1989).
- Truini, A. & Cruccu, G. Pathophysiological mechanisms of neuropathic pain. *Neurological sciences: official journal of the Italian Neurological Society and of the Italian Society of Clinical Neurophysiology* **27**(Suppl 2), S179–182, doi:<https://doi.org/10.1007/s10072-006-0597-8> (2006).
- Costigan, M., Scholz, J. & Woolf, C. J. Neuropathic pain: a maladaptive response of the nervous system to damage. *Annual review of neuroscience* **32**, 1–32, doi:<https://doi.org/10.1146/annurev.neuro.051508.135531> (2009).
- Llorens, C., Martres, M. P., Baudry, M. & Schwartz, J. C. Hypersensitivity to noradrenaline in cortex after chronic morphine: relevance to tolerance and dependence. *Nature* **274**, 603–605 (1978).
- Christie, M. J. & Overstreet, D. H. Sensitivity of morphine-tolerant rats to muscarinic and dopaminergic agonists: relation to tolerance or withdrawal. *Psychopharmacology* **65**, 27–34 (1979).
- Li, Q. *et al.* Disrupted Default Mode Network and Basal Craving in Male Heroin-Dependent Individuals: A Resting-State fMRI Study. *The Journal of clinical psychiatry* **77**, e1211–e1217, doi:<https://doi.org/10.4088/JCP.15m09965> (2016).
- Kleber, H. D., Topazian, M., Gaspari, J., Riordan, C. E. & Kosten, T. Clonidine and Naltrexone in the Outpatient Treatment of Heroin Withdrawal. *The American Journal of Drug and Alcohol Abuse* **13**, 1–17, doi:<https://doi.org/10.3109/00952998709001497> (1987).

16. Weintraub, Z., Bental, Y., Olivan, A. & Rotschild, A. Neonatal withdrawal syndrome and behavioral effects produced by maternal drug use. *Addiction biology* **3**, 159–170, doi:<https://doi.org/10.1080/13556219872227> (1998).
17. Bassett, D. S. & Sporns, O. Network neuroscience. *Nature neuroscience* **20**, 353–364, doi:<https://doi.org/10.1038/nn.4502> (2017).
18. Nucifora, P. G., Verma, R., Lee, S. K. & Melhem, E. R. Diffusion-tensor MR imaging and tractography: exploring brain microstructure and connectivity. *Radiology* **245**, 367–384, doi:<https://doi.org/10.1148/radiol.2452060445> (2007).
19. Skudlarski, P. *et al.* Measuring brain connectivity: diffusion tensor imaging validates resting state temporal correlations. *NeuroImage* **43**, 554–561, doi:<https://doi.org/10.1016/j.neuroimage.2008.07.063> (2008).
20. Clayden, J. D. Imaging connectivity: MRI and the structural networks of the brain. *Functional neurology* **28**, 197–203, doi:<https://doi.org/10.11138/FNeur/2013.28.3.197> (2013).
21. Briggman, K. L. & Denk, W. Towards neural circuit reconstruction with volume electron microscopy techniques. *Current opinion in neurobiology* **16**, 562–570, doi:<https://doi.org/10.1016/j.conb.2006.08.010> (2006).
22. Chklovskii, D. B., Vitaladevuni, S. & Scheffer, L. K. Semi-automated reconstruction of neural circuits using electron microscopy. *Current opinion in neurobiology* **20**, 667–675, doi:<https://doi.org/10.1016/j.conb.2010.08.002> (2010).
23. Briggman, K. L. & Bock, D. D. Volume electron microscopy for neuronal circuit reconstruction. *Current opinion in neurobiology* **22**, 154–161, doi:<https://doi.org/10.1016/j.conb.2011.10.022> (2012).
24. Kasthuri, N. *et al.* Saturated Reconstruction of a Volume of Neocortex. *Cell* **162**, 648–661, doi:<https://doi.org/10.1016/j.cell.2015.06.054> (2015).
25. Greicius, M. Resting-state functional connectivity in neuropsychiatric disorders. *Current opinion in neurology* **21**, 424–430 (2008).
26. Sheline, Y. I., Price, J. L., Yan, Z. & Mintun, M. A. Resting-state functional MRI in depression unmasks increased connectivity between networks via the dorsal nexus. *Proceedings of the National Academy of Sciences* **107**, 11020–11025 (2010).
27. Richards, T. L. & Berninger, V. W. Abnormal fMRI connectivity in children with dyslexia during a phoneme task: Before but not after treatment. *Journal of neurolinguistics* **21**, 294–304 (2008).
28. Koshino, H. *et al.* Functional connectivity in an fMRI working memory task in high-functioning autism. *NeuroImage* **24**, 810–821 (2005).
29. Jeong, J., Gore, J. C. & Peterson, B. S. Mutual information analysis of the EEG in patients with Alzheimer's disease. *Clinical neurophysiology: official journal of the International Federation of Clinical Neurophysiology* **112**, 827–835 (2001).
30. Peters, J. M. *et al.* Brain functional networks in syndromic and non-syndromic autism: a graph theoretical study of EEG connectivity. *BMC medicine* **11**, 54 (2013).
31. Brookes, M. J. *et al.* Measuring functional connectivity using MEG: methodology and comparison with fMRI. *NeuroImage* **56**, 1082–1104 (2011).
32. Alonso, J. F. *et al.* MEG connectivity analysis in patients with Alzheimer's disease using cross mutual information and spectral coherence. *Annals of biomedical engineering* **39**, 524–536 (2011).
33. Garofalo, M., Nieuws, T., Massobrio, P. & Martinoia, S. Evaluation of the performance of information theory-based methods and cross-correlation to estimate the functional connectivity in cortical networks. *PloS one* **4**, e6482, doi:<https://doi.org/10.1371/journal.pone.0006482> (2009).
34. Erickson, J., Tooker, A., Tai, Y.-C. & Pine, J. Caged neuron MEAs: A system for long-term investigation of cultured neural network connectivity. *Journal of neuroscience methods* **175**, 1–16 (2008).
35. Gong, X. W., Li, J. B., Lu, Q. C., Liang, P. J. & Zhang, P. M. Effective connectivity of hippocampal neural network and its alteration in Mg²⁺ -free epilepsy model. *PloS one* **9**, e92961, doi:<https://doi.org/10.1371/journal.pone.0092961> (2014).
36. Guzman, S. J., Schlogl, A., Frotscher, M. & Jonas, P. Synaptic mechanisms of pattern completion in the hippocampal CA3 network. *Science* **353**, 1117–1123, doi:<https://doi.org/10.1126/science.aaf1836> (2016).
37. Stetter, O., Battaglia, D., Soriano, J. & Geisel, T. Model-free reconstruction of excitatory neuronal connectivity from calcium imaging signals. *PLoS computational biology* **8**, e1002653, doi:<https://doi.org/10.1371/journal.pcbi.1002653> (2012).
38. Mishchencko, Y., Vogelstein, J. T. & Paninski, L. A Bayesian approach for inferring neuronal connectivity from calcium fluorescent imaging data. *The Annals of Applied Statistics*, 1229–1261 (2011).
39. Goveas, J. S. *et al.* Recovery of hippocampal network connectivity correlates with cognitive improvement in mild Alzheimer's disease patients treated with donepezil assessed by resting-state fMRI. *Journal of magnetic resonance imaging: JMIR* **34**, 764–773, doi:<https://doi.org/10.1002/jmri.22662> (2011).
40. Zhou, J. *et al.* Divergent network connectivity changes in behavioural variant frontotemporal dementia and Alzheimer's disease. *Brain: a journal of neurology* **133**, 1352–1367, doi:<https://doi.org/10.1093/brain/awq075> (2010).
41. Charkhkar, H. *et al.* Amyloid beta modulation of neuronal network activity *in vitro*. *Brain research* **1629**, 1–9, doi:<https://doi.org/10.1016/j.brainres.2015.09.036> (2015).
42. Galantucci, S. *et al.* Structural Brain Connectome and Cognitive Impairment in Parkinson Disease. *Radiology*, 160274, doi:<https://doi.org/10.1148/radiol.2016160274> (2016).
43. Jafri, M. J., Pearson, G. D., Stevens, M. & Calhoun, V. D. A method for functional network connectivity among spatially independent resting-state components in schizophrenia. *NeuroImage* **39**, 1666–1681, doi:<https://doi.org/10.1016/j.neuroimage.2007.11.001> (2008).
44. Zhang, J. *et al.* Disrupted brain connectivity networks in drug-naive, first-episode major depressive disorder. *Biological psychiatry* **70**, 334–342, doi:<https://doi.org/10.1016/j.biopsych.2011.05.018> (2011).
45. Greicius, M. D. *et al.* Resting-state functional connectivity in major depression: abnormally increased contributions from subgenual cingulate cortex and thalamus. *Biological psychiatry* **62**, 429–437 (2007).
46. Cooney, R. E., Joermann, J., Eugene, F., Dennis, E. L. & Gotlib, I. H. Neural correlates of rumination in depression. *Cognitive, affective & behavioral neuroscience* **10**, 470–478, doi:<https://doi.org/10.3758/CABN.10.4.470> (2010).
47. Wilke, C., Worrell, G. & He, B. Graph analysis of epileptogenic networks in human partial epilepsy. *Epilepsia* **52**, 84–93, doi:<https://doi.org/10.1111/j.1528-1167.2010.02785.x> (2011).
48. Canals, I. *et al.* Activity and High-Order Effective Connectivity Alterations in Sanfilippo C Patient-Specific Neuronal Networks. *Stem cell reports* **5**, 546–557, doi:<https://doi.org/10.1016/j.stemcr.2015.08.016> (2015).
49. Xu, J., Liu, Z.-r, Liu, R. & Yang, Q.-f Information transmission in human cerebral cortex. *Physica D: Nonlinear Phenomena* **106**, 363–374 (1997).
50. Lungarella, M., Pitti, A. & Kuniyoshi, Y. Information transfer at multiple scales. *Physical Review E* **76**, 056117 (2007).
51. Schreiber, T. Measuring information transfer. *Physical review letters* **85**, 461–464, doi:<https://doi.org/10.1103/PhysRevLett.85.461> (2000).
52. Barabási, A.-L. (Basic Books, 2002).
53. Rubinov, M. & Sporns, O. Complex network measures of brain connectivity: uses and interpretations. *NeuroImage* **52**, 1059–1069, doi:<https://doi.org/10.1016/j.neuroimage.2009.10.003> (2010).
54. Jiang, L., Xu, H. & Yu, C. Brain connectivity plasticity in the motor network after ischemic stroke. *Neural plasticity* **2013**, 924192, doi:<https://doi.org/10.1155/2013/924192> (2013).
55. Westlake, K. P. & Nagarajan, S. S. Functional connectivity in relation to motor performance and recovery after stroke. *Frontiers in systems neuroscience* **5**, 8, doi:<https://doi.org/10.3389/fnsys.2011.00008> (2011).
56. Bajaj, S., Butler, A. J., Drake, D. & Dhamala, M. Brain effective connectivity during motor-imagery and execution following stroke and rehabilitation. *NeuroImage: Clinical* **8**, 572–582, doi:<https://doi.org/10.1016/j.nicl.2015.06.006> (2015).

57. Schulz, R. *et al.* Enhanced Effective Connectivity Between Primary Motor Cortex and Intraparietal Sulcus in Well-Recovered Stroke Patients. *Stroke* **47**, 482–489, doi:<https://doi.org/10.1161/STROKEAHA.115.011641> (2016).
58. Almeida, S. R. *et al.* Brain Connectivity and Functional Recovery in Patients With Ischemic Stroke. *Journal of neuroimaging: official journal of the American Society of Neuroimaging* **27**, 65–70, doi:<https://doi.org/10.1111/jon.12362> (2017).
59. Lefebvre, S. *et al.* Increased functional connectivity one week after motor learning and tDCS in stroke patients. *Neuroscience* **340**, 424–435, doi:<https://doi.org/10.1016/j.neuroscience.2016.10.066> (2017).
60. Ramsey, L. E. *et al.* Normalization of network connectivity in hemispatial neglect recovery. *Annals of neurology* **80**, 127–141, doi:<https://doi.org/10.1002/ana.24690> (2016).
61. Cao, L. *et al.* Intermittent theta burst stimulation modulates resting-state functional connectivity in the attention network and promotes behavioral recovery in patients with visual spatial neglect. *Neuroreport* **27**, 1261–1265, doi:<https://doi.org/10.1097/WNR.0000000000000689> (2016).
62. Bharath, R. D. *et al.* Recovery of resting brain connectivity ensuing mild traumatic brain injury. *Frontiers in human neuroscience* **9**, 513, doi:<https://doi.org/10.3389/fnhum.2015.00513> (2015).
63. Falletta Caravasso, C. *et al.* The Default Mode Network Connectivity Predicts Cognitive Recovery in Severe Acquired Brain Injured Patients: A Longitudinal Study. *Journal of neurotrauma* **33**, 1247–1262, doi:<https://doi.org/10.1089/neu.2015.4003> (2016).
64. Vassal, M. *et al.* Recovery of functional connectivity of the sensorimotor network after surgery for diffuse low-grade gliomas involving the supplementary motor area. *Journal of neurosurgery*, 1–10, doi:<https://doi.org/10.3171/2016.4.JNS152484> (2016).
65. Kirov, S. A. & Harris, K. M. Dendrites are more spiny on mature hippocampal neurons when synapses are inactivated. *Nature neuroscience* **2**, 878–883, doi:<https://doi.org/10.1038/13178> (1999).
66. Benson, D. L. & Cohen, P. A. Activity-independent segregation of excitatory and inhibitory synaptic terminals in cultured hippocampal neurons. *The Journal of neuroscience: the official journal of the Society for Neuroscience* **16**, 6424–6432 (1996).
67. Tillema, J. M. *et al.* In vivo detection of connectivity between cortical and white matter lesions in early MS. *Multiple sclerosis*, doi:<https://doi.org/10.1177/1352458516671027> (2016).
68. Dogonowski, A. M. *et al.* Recovery from an acute relapse is associated with changes in motor resting-state connectivity in multiple sclerosis. *Journal of neurology, neurosurgery, and psychiatry* **87**, 912–914, doi:<https://doi.org/10.1136/jnnp-2015-311375> (2016).
69. Tonnie, E. & Trushina, E. Oxidative Stress, Synaptic Dysfunction, and Alzheimer's Disease. *Journal of Alzheimer's disease: JAD*, doi:<https://doi.org/10.3233/JAD-161088> (2017).
70. Vai, B. *et al.* Catechol-O-methyltransferase Val(108/158)Met polymorphism affects fronto-limbic connectivity during emotional processing in bipolar disorder. *European psychiatry: the journal of the Association of European Psychiatrists* **41**, 53–59, doi:<https://doi.org/10.1016/j.eurpsy.2016.10.002> (2016).
71. Vai, B. *et al.* Fronto-limbic effective connectivity as possible predictor of antidepressant response to SSRI administration. *European neuropsychopharmacology: the journal of the European College of Neuropsychopharmacology* **26**, 2000–2010, doi:<https://doi.org/10.1016/j.euroneuro.2016.09.640> (2016).
72. Fang, Z. *et al.* Serotonin transporter genotype modulates functional connectivity between amygdala and PCC/PCu during mood recovery. *Frontiers in human neuroscience* **7**, 704, doi:<https://doi.org/10.3389/fnhum.2013.00704> (2013).
73. Zakiniaez, Y., Scheinost, D., Seo, D., Sinha, R. & Constable, R. T. Cingulate cortex functional connectivity predicts future relapse in alcohol dependent individuals. *NeuroImage. Clinical* **13**, 181–187, doi:<https://doi.org/10.1016/j.nicl.2016.10.019> (2017).
74. Wasser, C. R. & Kavalali, E. T. Leaky synapses: regulation of spontaneous neurotransmission in central synapses. *Neuroscience* **158**, 177–188, doi:<https://doi.org/10.1016/j.neuroscience.2008.03.028> (2009).
75. Ramirez, D. M. & Kavalali, E. T. Differential regulation of spontaneous and evoked neurotransmitter release at central synapses. *Current opinion in neurobiology* **21**, 275–282, doi:<https://doi.org/10.1016/j.conb.2011.01.007> (2011).
76. Bossuyt, P. M. *et al.* STARD 2015: an updated list of essential items for reporting diagnostic accuracy studies. *Bmj* **351**, h5527, doi:<https://doi.org/10.1136/bmj.h5527> (2015).
77. DFG. in *Sicherung Guter Wissenschaftlicher Praxis* 1–109 (Wiley-VCH Verlag GmbH & Co. KGaA, 2013).
78. Welzel, O. *et al.* Synapse clusters are preferentially formed by synapses with large recycling pool sizes. *PLoS one* **5**, e13514, doi:<https://doi.org/10.1371/journal.pone.0013514> (2010).
79. Tischbirek, C. H. *et al.* Use-dependent inhibition of synaptic transmission by the secretion of intravesicularly accumulated antipsychotic drugs. *Neuron* **74**, 830–844, doi:<https://doi.org/10.1016/j.neuron.2012.04.019> (2012).
80. Sbalzarini, I. F. & Koumoutsakos, P. Feature point tracking and trajectory analysis for video imaging in cell biology. *Journal of structural biology* **151**, 182–195, doi:<https://doi.org/10.1016/j.jsb.2005.06.002> (2005).
81. Jia, H., Rochefort, N. L., Chen, X. & Konnerth, A. In vivo two-photon imaging of sensory-evoked dendritic calcium signals in cortical neurons. *Nature protocols* **6**, 28–35, doi:<https://doi.org/10.1038/nprot.2010.169> (2011).
82. Deneux, T. *et al.* Accurate spike estimation from noisy calcium signals for ultrafast three-dimensional imaging of large neuronal populations in vivo. *Nature communications* **7**, 12190, doi:<https://doi.org/10.1038/ncomms12190> (2016).
83. Salinas, E. & Sejnowski, T. J. Correlated neuronal activity and the flow of neural information. *Nature reviews. Neuroscience* **2**, 539–550, doi:<https://doi.org/10.1038/35086012> (2001).
84. Seiffert, C., Khoshgoftaar, T. M., Van Hulse, J. & Napolitano, A. RUSBoost: A hybrid approach to alleviating class imbalance. *IEEE Transactions on Systems, Man, and Cybernetics-Part A: Systems and Humans* **40**, 185–197 (2010).

Acknowledgements

J.K.W., M.D. and T.W.G. were supported by a grant from the Else Kröner-Fresenius Foundation (2012_A35). We are deeply grateful to everybody who contributed to this work. Especially, we thank Katrin Ebert and Sandra Rittig for their excellent technical support.

Author Contributions

J.K.W. conceptualized the study, programmed the analysis software scripts and simulations, performed live cell recordings, analyzed the data – including investigation, methodology, formal analysis and validation. She wrote the original draft and reviewed and edited the manuscript and was responsible for the data curation, visualization and project administration. She also supervised M.D. in performing experiments. V.v.E. programmed the transfer entropy and generalized transfer entropy software functions, and K.B. supervised V.v.E. in programming these functions. M.D. performed live cell recordings. A.M. and J.K. provided the resources necessary for this work. T.W.G. conceptualized the study, supervised J.K.W., proof-read and helped revise the manuscript. The present work was performed by J.K.W. in partial fulfillment of the requirements for her obtaining the degree “Dr. rer. biol. hum.” at the University of Erlangen-Nuremberg. All authors contributed to the preparation of the final manuscript and lend shape to the final version.

Additional Information

Supplementary information accompanies this paper at doi:[10.1038/s41598-017-11729-5](https://doi.org/10.1038/s41598-017-11729-5)

Competing Interests: The authors declare that they have no competing interests.

Publisher's note: Springer Nature remains neutral with regard to jurisdictional claims in published maps and institutional affiliations.



Open Access This article is licensed under a Creative Commons Attribution 4.0 International License, which permits use, sharing, adaptation, distribution and reproduction in any medium or format, as long as you give appropriate credit to the original author(s) and the source, provide a link to the Creative Commons license, and indicate if changes were made. The images or other third party material in this article are included in the article's Creative Commons license, unless indicated otherwise in a credit line to the material. If material is not included in the article's Creative Commons license and your intended use is not permitted by statutory regulation or exceeds the permitted use, you will need to obtain permission directly from the copyright holder. To view a copy of this license, visit <http://creativecommons.org/licenses/by/4.0/>.

© The Author(s) 2017